ACS APPLIED BIO MATERIALS

www.acsabm.org
Article

Collagen Hybridizing Peptides Promote Collagen Fibril Growth *In Vitro*

Sophia Huang,* Nicole Ng, Mina Vaez, Boris Hinz, Iona Leong, and Laurent Bozec

Cite This: *ACS Appl. Bio Mater.* 2025, 8, 2003−2014
Read Online

ABSTRACT: Recreating the structural and mechanical properties of native tissues *in vitro* presents significant challenges, particularly in mimicking the dense fibrillar network of extracellular matrixes such as skin and tendons. This study develops a reversible collagen film through cycling collagen self-assembly and disassembly, offering an innovative approach to address these challenges. We first generated an engineered collagen scaffold by applying plastic compression to the collagen hydrogel. The reversibility of the collagen assembly was explored by treating the scaffold with lactic acid, leading to its breakdown into an amorphous gel—a process termed defibrillogenesis. Subsequent immersion of this gel in phosphate buffer facilitated the reassembly of collagen into fibrils larger than those in the original scaffold yet with the D-banding pattern characteristic of collagen fibrils. Transfer learning of the mobileNetV2 convolutional neural network trained on atomic force microscope images of collagen nanoscale D-banding patterns was created with 99% training and testing accuracy. In addition, extensive external validation was performed, and the model achieved high robustness and generalization with unseen data sets. Further innovation was introduced by applying collagen hybridizing peptides, which significantly accelerated and directed the assembly of collagen fibrils, promoting a more organized and aligned fibrillar structure. This study not only demonstrates the feasibility of creating a reversible collagen film that closely mimics the density and structural properties of the native matrix but also highlights the potential of using collagen hybridizing peptides to control and enhance collagen fibrillogenesis. Our findings offer promising tissue engineering and regenerative medicine strategies by enabling precise manipulation of collagen structures *in vitro*.

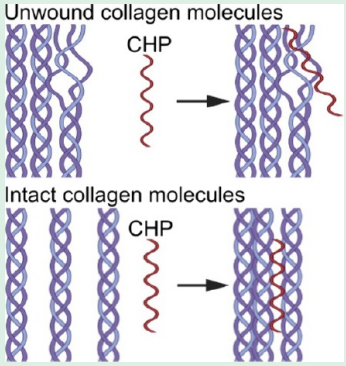

KEYWORDS: *collagen, fibrillogenesis, peptide, CHP, CMP, atomic force microscopy*

INTRODUCTION

The extracellular matrix (ECM) is a complex network of proteins and carbohydrates that provides structural and biochemical support to cells within tissues and organs.[1] Collagen is the most abundant protein in the ECM of many tissues, including skin, bone, and cartilage.[2] The foundational units of collagen are triple helix molecules, which comprise three α-helical polypeptide chains that supercoil into the triple helix.[3] One triple helix is typically 300 nm long and 1.5 nm in diameter[4] and undergoes self-assembly with other helices into collagen fibrils via electrostatic and hydrophobic interaction.[5] A hallmark of type I collagen self-assembly is the characteristic 67 nm repeating pattern of dark and light bands observed in electron micrographs of collagen fibrils, called D-banding.[6] According to the Hodge−Petruska model, these bands result from collagen molecules organized in a quarter-stagger arrangement.[7] This characteristic pattern is conserved across all tissues and species, and it is commonly used as a structural marker to identify collagen fibrils at the nanoscale.[8] Collagen hydrogels are the most widely used *in vitro* representation of the ECM for studying cell behavior, tissue development, and disease progression.[9] Most collagen hydrogels are porous because of the low density of collagen fibrils and thus do not accurately represent the collagen density of the ECM.

Collagen-based biomaterial functions beyond the representation of ECM; other applications include drug delivery systems, implantable devices, and tissue repair and regeneration.[10] However, collagen material derived from natural animal sources carries risks such as allergic reactions and pathogen transfer.[11] The lab-based engineered collagen has the advantages of being flexible in design, free of pathogens, biocompatible, and biodegradable.[12] Thus, lab-based engineered collagen is ideal in diverse wound healing applications, such as sutures, skin replacement for burned patients, or cardiac valves.[13] Strategies to produce lab-based engineered collagen include cell-produced collagen, recombinant collagen, and synthetic collagen.[14] Over the past decade, synthetic

Received: October 15, 2024
Revised: January 30, 2025
Accepted: February 6, 2025
Published: February 26, 2025

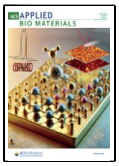

collagen has gained traction and success in generating biomimetic collagen,[15] but it has yet to be used to support lab-based collagen engineering.

Collagen mimetic peptide (CMP) is a synthetic collagen that mimics natural collagen's amino acid sequence, structure, and bioactivity.[16] Given that the most prevalent amino acid sequence in collagen is Pro-Hyp-Gly, the most studied CMP sequence often involves repeats of $(Pro\text{-}Hyp\text{-}Gly)_n$.[16] Like natural collagen, CMP can self-assemble to form a triple helix, which can further assemble into nanofiber and hydrogel through complementary sticky-ended assembly mechanisms.[17] However, the nanofibers formed from synthetic CMP are about 10 nm long, whereas natural collagen molecules can span over 300 nm in length.[18] Thus, much work remains to explore how such short, disorganized CMP could form or contribute to forming a highly organized collagen fibril structure closely resembling the ECM. Within the field of CMPs, collagen hybridizing peptide (CHP) is the only commercially available CMP comprising 6−10 repeat units of Pro-Hyp-Gly with a fluorophore, such as Cy3 or 5-FAM, attached to the end of the peptide.[19] CHP can spontaneously hybridize with unwound collagen triple helix and detect damage in collagen-rich tissue.[20] For example, CHP can detect collagen damage in thermally injured human skin,[21] idiopathic pulmonary fibrosis,[22] and wound healing.[23] However, to date, CHP has been used as a detection tool only for damaged collagen; no study has explored how CHP could impact the formation of collagen fibrils.

Herein, we establish a high-density collagen environment that closely resembles the collagen density found in the native tissue. Our focus is to assess the impact of CHP on collagen fibril formation within this high-density collagen setting, with the overarching goal of fabricating a collagen fibril network that closely mimics the structural characteristics of the native ECM. Here, we create the high-density collagen film by cycling collagen self-assembly and disassembly, introduce CHP to the reversible collagen film, and demonstrate that CHP can accelerate the fibril assembly process and generate a highly aligned collagen fibril network with structural properties that resemble the native ECM. Our findings could lead to possible biomimetic collagen material toward therapeutic avenues for rapid tissue regeneration in wound healing applications.

METHODS

Collagen Scaffolds Engineering Protocol. Collagen scaffolds were prepared by mixing 10 mL of rat-tail tendon collagen type I solution (2.0 mg/mL collagen protein in 0.6% acetic acid; First Link Ltd., UK) with 1 mL of 10X Eagle's minimum essential medium (MEM). The solution was neutralized to pH 7.2 using 5 M NaOH and 1 M acetic acid (200 μL in total). The density of the collagen hydrogel $\rho_{\text{collagen hydrogel}}$ = 1.78 mg/mL (20 mg collagen in 11.2 mL solution). Here, 1 mL of the neutralized solution was aliquoted into each well of a 24-well plate (each well is 16 mm in diameter) and incubated in a 37 °C incubator for 30 min. The collagen hydrogels were then plastically compressed to increase their density using a modified protocol from Brown et al.[24] Following compression, the scaffolds were stored in phosphate-buffered saline (PBS) at 4 °C until use (<7 days). A 4 mm biopsy puncher was used to standardize the size of the collagen scaffold and physisorbed onto a glass slide by keeping the scaffold at room temperature until thoroughly dried. The resultant air-dried plastic compressed collagen gel is named engineered collagen scaffolds (ECS). The density of ECS ρ_{ECS} = mass/volume = 0.74 mg/mm^3 (mass m_{ECS} = 1.78 mg/mL × 1 mL × (16 mm/4 mm) = 0.4 mg; volume v_{ECS} = circular base area × height = 12.6 mm^2 × 0.043 mm = 0.54 mm^3).

Reverse-Fibrillogenesis Protocol. Glacial acetic acid (Sigma-Aldrich, US, 17.4 M) and lactic acid stock solution (Sigma-Aldrich, US, 11.3 M) were diluted to reach 100 mM solutions with respective pH = 2.35 for the lactic acid solution and pH = 2.88 for the acetic acid solution. The physisorbed collagen scaffolds were exposed to either acidic solution (1 mL) for 8 min. This optimum degradation time was defined as when the collagen fibrils no longer displayed any D-banding periodicity using an atomic force microscope (AFM) (5 images taken randomly to confirm; image acquisition protocol refers to Atomic Force Microscope Image Acquisition) and was determined through a titration pilot study of acid concentration vs degradation time. The samples were then rinsed gently in a Milli-Q (pH = 7) water bath immersion for 10 min to remove the bulk of the acid solution within the sample. Once removed from the water bath, a further 200 μL of Milli-Q water (pH = 7) was deposited on the acid-degraded collagen scaffolds to buffer the remaining acid solution within the scaffold that may not have been washed away. All acid-degraded collagen scaffolds were left to dry slowly overnight at room temperature before being stored at 4 °C until use (<7 days).

The reverse-fibrillogenesis of the collagen scaffold postacid degradation was achieved by immersing the acid-degraded collagen film in 1 mL PBS for 24 h, followed by a 10 min rinse in Milli-Q water. All reformed collagen scaffolds were left to dry at room temperature before being stored at 4 °C until use (<7 days).

CHP Staining Protocol. A stock solution of 100 μM R-CHP (3helix, Salt Lake City, Utah, US) was prepared by dissolving the CHP powder in 1 mL of PBS. This CHP contains a fluorescent reporter Cy3, rendering its localization possible by fluorescence. In our approach, 1 μM CHP solutions were diluted with PBS and heated to 80 °C for 5 min to disassociate the CHP triple helix to single peptides that can bind to damaged collagen (following manufacturer's protocol). As recommended by the protocol, the heated CHP solution was then cooled in ice for 1 min to avoid any thermal damage to tissue during staining. Here, 50 μL of CHP solution was pipetted directly onto the surface acid-degraded collagen film to cover the collagen film entirely and left to stain the sample for 8 h at 4 °C or 2 h at room temperature (depending on experimental conditions). After staining, the slides were rinsed with PBS for 5 min, followed by 2 rinses of Milli-Q water for 5 min before being left to air-dried at room temperature. The samples were finally stored at 4 °C until use (<7 days).

For live time-lapse imaging of the fibrils, the samples were mounted directly within a dedicated 3D-printed liquid holder and immersed in 400 μL of either PBS or 1 μM CHP solution. The samples were kept at room temperature.

Atomic Force Microscope Image Acquisition. A JPK AFM instrument (JPK Nanowizard@4 BioScience, Germany) was used to image the collagen fibrils and scaffolds. Collagen imaging was performed in contact mode under ambient conditions using a MSLN-10-D instrument (Bruker, Germany). Here, 10 μm ×10 μm images were typically recorded with optimized settings at 1.5 Hz scanning rate. All images were processed, and data analysis was performed using the JPK data processing software (version 6.3.5).

Bright-Field and Fluorescent Image Acquisition. A Zeiss Axio Observer 7 inverted confocal microscope equipped with an LSM 800 scan head and ZEN software (Zeiss, Germany) was used to acquire the CHP-mediated collagen growth under bright-field and Cy3 fluorescent. The Plan Apochromat objectives used were Zeiss 20× (Plan Apochromat; 20 × /0.8). The same microscope setup was also used to capture the live growth video of CHP and PBS-mediated collagen growth with a reversible collagen film. A dedicated 3D-printed liquid holder was designed to house the collagen scaffold during image acquisition and to prevent buffer evaporation during time-lapse acquisition. Images were captured every 5 min for 3 h for the CHP-stained scaffolds and every 10 min for 12 h for the PBS control samples.

Second Harmonic Generation Microscope Image Acquisition. The second harmonic generation images were acquired with a Nikon A1R HD MP+ multiphoton Imaging System (CF175 Apochromat; 25 × /1.10 NA; 2.0 mm WD; water) equipped with

https://doi.org/10.1021/acsabm.4c01509
ACS Appl. Bio Mater. 2025, 8, 2003−2014

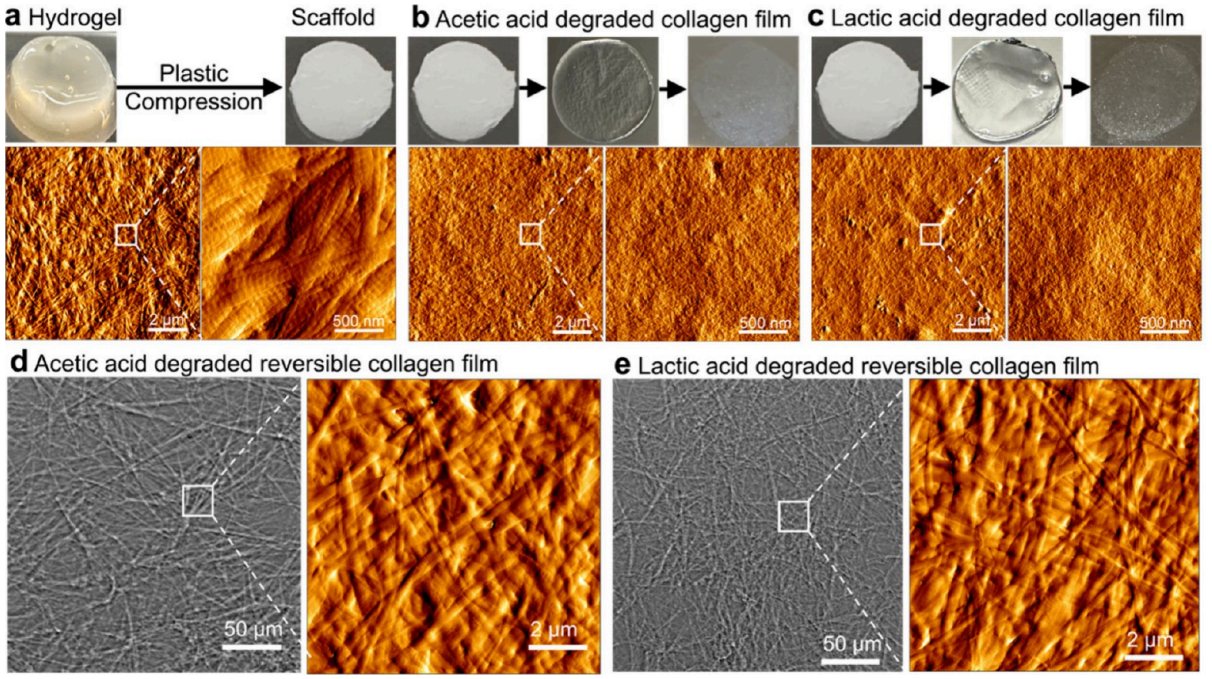

Figure 1. Cycling collagen self-assembly process to create reversible collagen film. (a) Plastic compression on collagen hydrogel creates a high-density engineered collagen scaffold (ECS) with well-defined collagen fibrils. (b) Acetic acid degradation of ECS creates an amorphous collagen film. The photo on the left is ECS. The middle photo is acetic acid degraded collagen film before air-dry, and the right photo is air-dried AA = RCF. (c) Lactic acid degradation of ECS creates amorphous collagen film. The photo on the left is ECS. The middle photo is lactic acid degraded collagen film before air-dry, and the right photo is air-dried LA = RCF. (d) Submerge the acetic acid degraded collagen film in PBS results in fibril reformation. (e) Submerge the lactic acid degraded collagen film in PBS results in fibril reformation.

Nikon halogen illumination and NIS-Elements Advanced Research software following a previously developed protocol from Chen et al.[25]

Convolutional Neural Network Model Training and Evaluation. The collagen D-banding data set consisted of 50 AFM images of plastic-compressed collagen scaffolds and 50 AFM images of lactic acid-degraded collagen scaffolds acquired by JPK Nanowizard4 AFM. Each AFM image was standardized at 10 μm × 10 μm (512 × 512 pixels). Each AFM image was further segmented following a 10 × 10 grid, generating 100 1 μm × 1 μm subimages per one AFM image (Figure 2a). Thus, 5000 images of the plastic-compressed collagen scaffold were obtained and labeled as "D-banding", and 5000 images of lactic acid-degraded collagen scaffold were obtained and labeled as "no D-banding".

The pretrained MobileNetV2 convolutional neural network (CNN) models were selected for the collagen D-banding data set, split into 70% training, 10% validation, and 20% testing. The training process utilized a cross-entropy loss function, stochastic gradient descent optimizer, and a learning rate of 0.001.

The model performance was evaluated with an accuracy curve, precision, recall, F1 score, confusion matrix, and Mathew's correlation coefficient. External data sets were also included to test the model's robustness and generalizability. To visualize the model's recognition result on the external data set (performed on data sets not used for training or validation), the recognition output was displayed as a green or red box overlaying the AFM images, in which the green box means the trained model recognizes the area as "D-banding", and the red box means the model recognizes the area as "no D-banding".

Computational Environment. The CNN model was trained using a MacBook Pro 14 in. laptop (2021), with macOS Ventura version 13.2.1, Apple M1 pro chip with 10-core CPU and 16-core GPU, and 16GB Unified Memory. Pytorch-GPU was employed to build the network architecture. Training was performed in Python 3.10 by using the Pycharm community virtual environment.

Image Analysis. Python was used for all of the optical image analyses. Packages used include cv2, numpy, os, and pandas. The image processing includes grayscale conversion, Gaussian blur, canny edge detection, and Hough lines identification.

Statistical Analysis. GraphPad Prism9 was used for graph plotting, and the nonpaired t test was used for statistical analysis. $P < 0.01$ is considered significant.

Code Availability. The code for training the ColD model and generating recognition results is provided at https://github.com/SophiaSXH/ColD-Model.git.

Model weights for ColD can be assessed for academic research purposes at https://huggingface.co/SophiaxHuang/ColD.

RESULTS

Acid Degradation of Collagen Scaffold to Create Amorphous Collagen Film. Collagen hydrogels frequently serve as *in vitro* representations of the ECM.[26] Yet, the collagen fibrils' density in these hydrogels is significantly lower than that of native tissue such as tendons or skin, thus not accurately representing ECM structural and mechanical properties. We used plastic compression on the collagen hydrogel to increase the collagen scaffold density (Figure 1a).[24] Previous work has demonstrated that the collagen scaffold will not reswell or reabsorb the water if stored in aqueous environments.[27] After air drying, the resulting ECS (defined as compressed and air-dried collagen scaffold) had a dense sheet appearance (Figure 1a), which is well documented for this type of collagen production.[28] The height of the uncompressed collagen hydrogel was 0.85 mm (n = 30), and the height of the compressed air-dried ECS was 0.043 mm (n = 30). Since no collagen is lost during plastic compression, we can calculate that the plastic compression method removed 95% of the water from the collagen hydrogel.

AFM was used to image the ECS at the nanoscale to characterize the collagen fibril morphology and confirm the

https://doi.org/10.1021/acsabm.4c01509
ACS Appl. Bio Mater. 2025, 8, 2003−2014

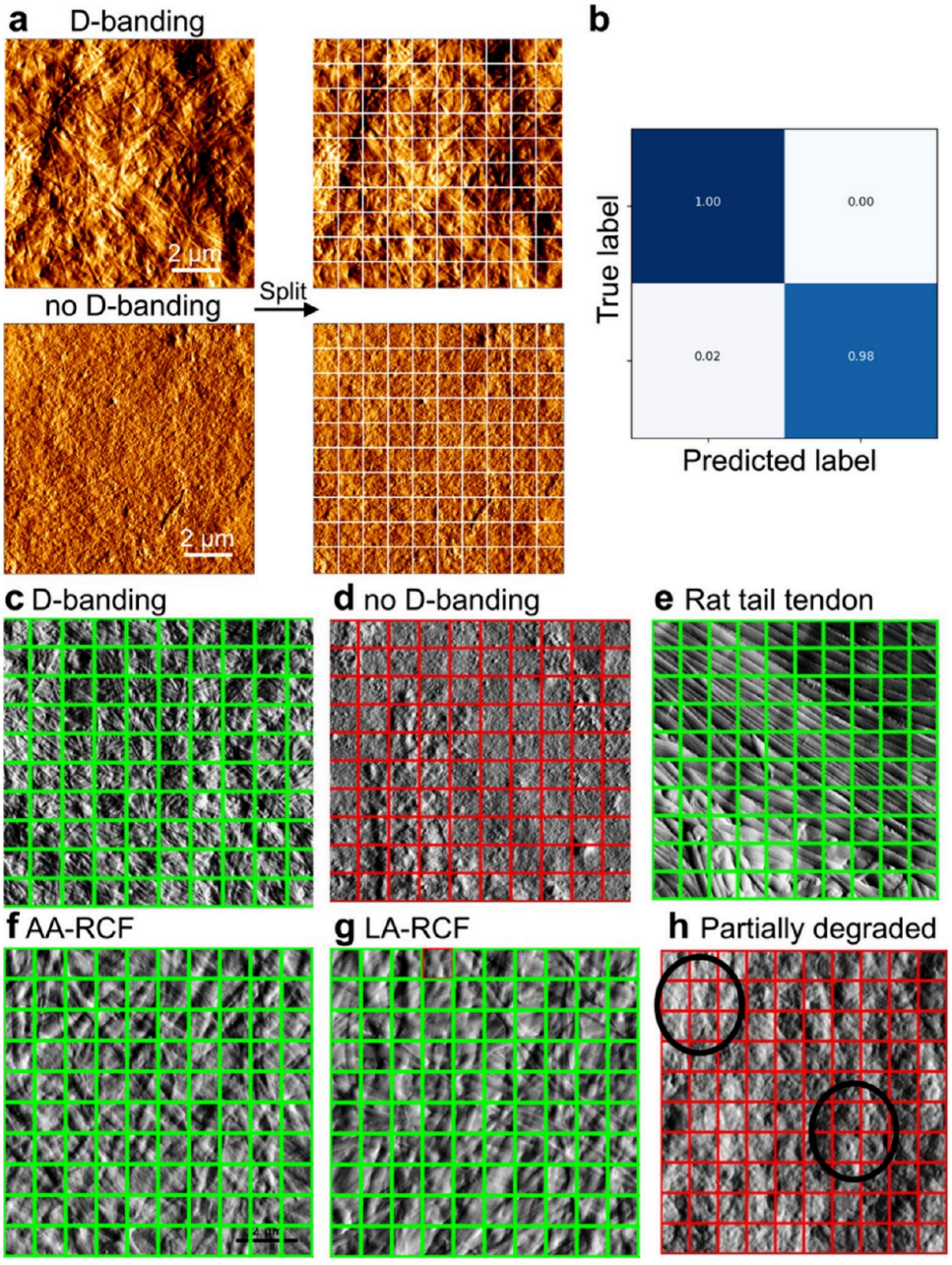

Figure 2. Utilizing convolutional neural network to recognize collagen D-banding pattern. (a) Training data set processing that split 50 AFM images of D-banding and 50 AFM images of no D-banding following a 10 × 10 grid, yielding 5000 AFM images of D-banding and 5000 images of no D-banding used in training. (b) Confusion matrix of the training results with MobileNetV2. True positive = 1, false positive = 0, true negative = 0.98, false negative = 0.02. (c) External validation results on the D-banding image that was recognized as all yes. (d) External validation result on no D-banding image that was recognized as all no. (e) External validation result on rat tail tendon image was recognized as all yes. (f) External validation result on acetic acid degraded reversible collagen film (AA-RCF) image that was recognized as all yes. (g) External validation result on lactic acid degraded reversible collagen film (LA-RCF) image that was recognized as all yes. (h) External validation result on partially degraded collagen scaffold using a low concentration of lactic acid image was recognized as all no. Circles show collagen D-banding but not 67 nm recognized as no. Green box = D-banding; red box = no D-banding.

proper formation of collagen fibrils. The collagen scaffold presents a highly dense collagen fibril network with clearly defined fibrils with visible boundaries, edges with neighboring fibrils, and an apparent D-banding periodicity (Figure 1a). This highly dense collagen scaffold mimics the fibril density of native tissues such as skin with the characteristic D-banding periodicity (D) along the long axis of the collagen fibrils.[29] Here, we measured D = 67 ± 4 nm (n = 60), corresponding to the accepted D-banding periodicity value for type I collagen fibrils conserved across tissues and species.[30] The orientation of the fibrils within the ECS did not follow a predominant orientation, as the fibrils remain organized randomly postcompression.

The average fibril width in the ECS W_{ECS} = 143 ± 38 nm (n = 30), whereas collagen fibrils in tendon tissues (fibril diameter range from 80 to 300 nm[31]) are much larger than in the ECS. Collagen concentration is a known factor contributing to *in vitro* collagen fibrils size, in which a higher collagen

https://doi.org/10.1021/acsabm.4c01509
ACS Appl. Bio Mater. 2025, 8, 2003−2014

concentration can result in larger fibrils forming.[32] To better replicate the size of collagen fibrils found in living organisms, we theorized that using highly concentrated ECS instead of a liquid collagen stock solution for fibrillogenesis could lead to the formation of larger collagen fibrils *in vitro*. We achieve this by exposing the ECSs to acetic or lactic acid solutions to reverse collagen fibrillogenesis and create a highly dense, amorphous collagen film. Acetic acid is routinely used to disassemble collagen fibrils into single-molecule solutions and is widely used to extract and store collagen from animal sources.[33] Lactic acid is naturally produced during anaerobic metabolism and is known to increase the synthesis of type I collagen in the ECM.[34] At the macroscale, the dense sheet appearance of the ECS has disappeared following exposure to either acid giving rise to a transparent amorphous film reminiscent of gelatin[35] (Figure 1b, c). After air-drying, these amorphous collagen films were imaged by AFM, and we could not observe any collagen fibrils in the amorphous collagen films (Figure 1b, c).

This confirms that the fibrillar morphology of the ECSs observed before acid exposure has structurally disappeared, as they have undergone defibrillogenesis by breaking down into small fibrillar fragments and single molecules, as expected. The collagen fibril structures in the ECS are stabilized by weak dispersive interaction and hydrogen bonding without intermolecular covalent bonds or cross-links.[36] Because of these weak interactions, the self-assembly process can be reversed by changes in temperature, pH, or ionic strength,[37] causing defibrillogenesis or breakdown of the fibrils.

Cycling Collagen Self-Assembly Process to Create Reversible Collagen Film. The newly created collagen film contains densely packed, disassembled collagen fragments. To verify whether these disassembled collagen fragments in their solid state can reform into collagen fibrils and to test our hypothesis that high-density collagen can form larger fibrils, we immersed the acid-degraded collagen film in 100 μL of PBS for 24 h. The newly reformed collagen network exhibits dispersed large fibrils for both the acetic acid and lactic acid degraded film (Figure 1d, e), confirming that the self-assembly of collagen is entirely reversible and that this process is modulated by pH cycling. At the nanoscale, the reformed collagen fibrils from the acetic acid-degraded reversible collagen film (AA-RCF) had an average fibril width of $W_{AA\text{-}RCF}$ = 376 ± 99 nm (n = 30) (Figure 1d), and the lactic acid-degraded reversible collagen film (LA-RCF) had an average fibril width of $W_{LA\text{-}RCF}$ = 329 ± 130 nm (n = 30) (Figure 1e). These were significantly larger ($p < 0.0001$, t test) than the fibrils in the ECS: W_{ECS} = 143 ± 38 nm (n = 30). The reformed fibrils from both AA-RCF and LA-RCF also retained the 67 nm D-banding signatures measured as 67 ± 12 nm (n = 30), confirming that not only could the fibrils reform but they also reform with the structural arrangement of native type I collagen.

The density of the collagen hydrogel $\rho_{collagen\ hydrogel}$ = 1.78 mg/mL (1.78 mg/mL = 0.00178 mg/mm^3), and the density of ECS ρ_{ECS} = 0.74 mg/mm^3. In the case of the AA-RCF or LA-RCF, the height of the film was approximately 3 μm in thickness and 8 mm in diameter, which is 14 times thinner and double in diameter compared to the ECS (preacid degradation). We attribute the size change to the loss of collagen fibril structures. Even though the ECS is air-dried, it is not entirely dehydrated, and there are intrafibular and interfibular water molecules that remain in the ECS because ECS contains fully formed collagen fibrils. However, after acid degradation and air-drying, the loss of collagen fibrils and air-drying further dehydrates the collagen film, leading to a thinner and more expanded structure. Assuming that there was no collagen lost during the acid degradation of the ECS and air-drying process, the $\rho_{AA\text{-}RCF\ or\ LA\text{-}RCF}$ = 2.67 mg/mm^3 (mass $_{AA\text{-}RCF\ or\ LA\text{-}RCF}$ = m_{ECS} = 0.4 mg and volume $_{AA\text{-}RCF\ or\ LA\text{-}RCF}$ = circular base area × height = 50.24 mm^2 × 0.003 mm = 0.15 mm^3).

The reversible collagen film is approximately 3.6 times denser than the ECS and 1500 times denser than the collagen hydrogel. We attribute the significant increase (2.3-fold) in fibril width between ECS and RCF to the increased density of the collagen available for self-assembly, indicating that the collagen's preassembly density may play a role in determining the resultant collagen fibril width. Using the denser collagen film instead of a collagen stock solution for the collagen fibrillogenesis process, we doubled the collagen fibril size to over 300 nm, mimicking the size of tendon collagen fibril—the largest collagen fibril found in humans.

Utilizing Deep Learning to Recognize Collagen D-Banding Pattern. ECS and the reformed collagen macrofibrils contain well-defined collagen fibrils; however, to confirm the 67 nm D-banding pattern on each AFM image, we must manually measure the D-banding pattern size with image analysis software such as Gwyddion.[38] Manual measuring can be labor-intensive, mainly when dealing with hundreds of AFM images. CNN is the most widely used deep learning algorithm for image classification and computer vision tasks.[39,40] MobileNetV2 is a lightweight CNN model designed for computation and memory efficiency on mobile devices.[41] It contains depth-wise and point-wise convolutions to reduce the number of parameters compared to traditional convolutions.[41] Thus, the MobileNetV2 CNN model was chosen to automatically recognize collagen D-banding patterns on AFM images. The training data set consisted of 5000 1 μm × 1 μm AFM images of the ECS labeled as "D-banding" and 5000 1 μm × 1 μm AFM images of lactic acid-degraded collagen film labeled as "no D-banding" (Figure 2a). After 25 epochs (defined as a complete pass through the entire training data set), the MobileNetV2 model achieved 99.61% training accuracy, 99.1% test accuracy, 99.67% precision, 98.33% recall, 98.99% F1 score, and Mathew's correlation coefficient (MCC) is 98.19%. The confusion matrix indicates a 2% false positive rate of the model (Figure 2b).

Next, external data sets were used to test the collagen D-banding (ColD) model's robustness and generalizability. The external data sets contain AFM images not used in the training and testing processes and other collagen sources in which the fibril morphology differs from the training data set, but the D-banding is conserved. The ColD model performed very well on ECS images that are the same source as the training data set but never used for training. Results showed that the ColD model recognized the ECS as 100% "D-banding" (n = 1,00 1 μm × 1 μm images, accuracy 99.4%) (Figure 2c) and the acid-degraded collagen film as 100% "no D-banding" (n = 1000 1 μm × 1 μm images accuracy 99.6%) (Figure 2d). Similar performance was observed on rat tail tendon AFM images, in which the ColD model recognized the rat tail tendon collagen fibrils as 100% "D-banding" (n = 1000 1 μm × 1 μm images, accuracy 99.6%) (Figure 2e). The collagen fibrils in the rat tail tendon are wider $W_{rat\ tail\ tendon}$ = 519 ± 110 nm (n = 30) and more aligned than the collagen scaffold used in training, but

https://doi.org/10.1021/acsabm.4c01509
ACS Appl. Bio Mater. 2025, 8, 2003−2014

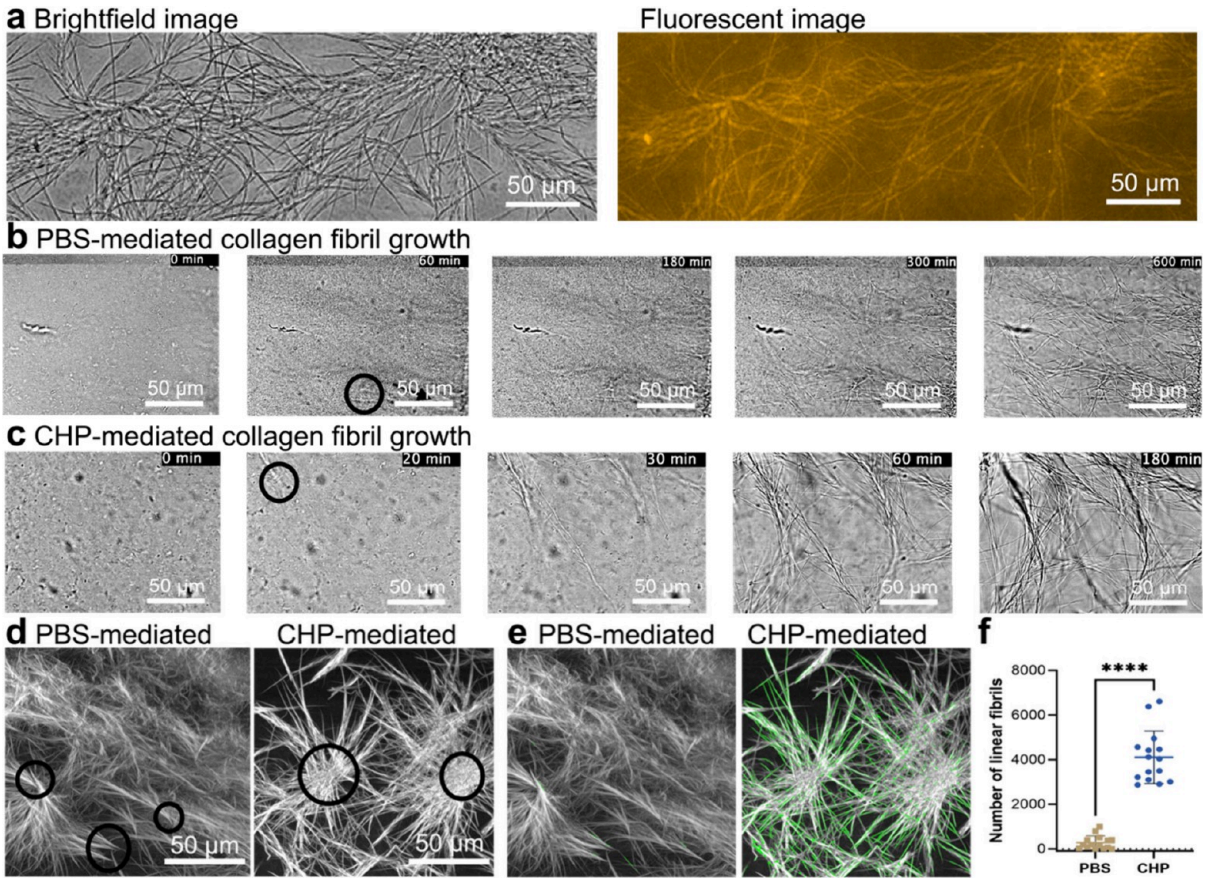

Figure 3. Collagen hybridizing peptide (CHP) mediated collagen fibril growth in high-density collagen film. (a) Bright-field and fluorescent images of CHP-mediated collagen fibril growth, images taken after fibrils are fully formed and air-dried. (b) Time-lapse imaging of PBS-mediated (control) collagen fibril growth (in liquid) with initial growth at 1 h and full growth after 8 h. (c) Time-lapse imaging of CHP-mediated collagen fibril growth (in liquid) with initial growth at 10 min and total growth after 2 h. (d) Second harmonic generation imaging of PBS-mediated collagen fibril growth (left) showing nucleation site (circles) and fibril growth in all directions and CHP-mediated collagen fibril growth (right) showing nucleation site (circles) and more directional growth from nucleation site. Images taken after fibrils are fully formed and air-dried. (e) Fibril linearity measurements of PBS-mediated growth (left) and CHP-mediated growth (right); linear fibrils are highlighted in green. (f) Quantification of linear fibrils between PBS and CHP-mediated fibril growth, $p < 0.0001$, nonpaired t test.

the D-banding pattern is conserved. The 100% "D-banding" result demonstrates that the ColD model can generalize well to unseen data sets when the collagen fibrils size and morphology have changed, but with the D-banding pattern conserved. The reformed collagen fibrils, when exposed to the AA-RCF and LA-RCF with PBS for 24 h, were also tested with the ColD model. The result showed that both reformed fibrils with double the fibril size from the training data set were recognized as D-banding (n = 1000 1 μm × 1 μm images, accuracy 98.6%) (Figure 2f, g). The 67 nm D-band pattern was also previously confirmed manually.

A more complex external data set for the validation is the partially degraded collagen scaffold, in which the ECS was degraded with low concentration lactic acid (1 mM lactic acid for 8 min), resulting in incomplete degradation of collagen fibrils. AFM images of the partially degraded collagen scaffold show that in some areas fragments of D-banding patterns can be observed (Figure 2h, circles), and in some areas, the collagen fibrils are completely degraded with no visible D-banding pattern. Even though the collagen D-banding pattern from a low concentration of acid degradation visually appeared to have the signature gap and overlap regions, the swelling and dissociation of the fibrils caused an increase in D-banding size, measured as 89 ± 17 nm (n = 30). Thus, a model that recognizes the 67 nm collagen D-banding pattern should not recognize the swelled D-banding as normal. The ColD model recognized the swelling D-banding as 0% "D-banding" (n = 1000 1 μm × 1 μm images, accuracy 99.6%), which suggests that it does not recognize another size of D-banding and only recognizes the 67 nm D-banding.

The external validation outcome demonstrated our ColD model's robust generalization on collagen D-banding pattern recognition. Combined with the 99% accuracy, we can conclude that the ColD model can accurately recognize the 67 nm D-banding pattern on any given AFM images of collagen fibrils.

Modulating Collagen Fibril Growth Using CHP. The collagen macrofibrils derived from the collagen film are randomly organized when submerged in PBS, unlike the native tissues such as skin, where the collagen fibrils align parallel to form bundles.[29] One of the mechanisms involved in the growth and organization of collagen fibrils *in vivo* is the alternation of charged and hydrophobic side chains on the surface of the helix, which is determined by the sequences of amino acids and the conditions under which fibrils form.[42] We hypothesized that adding extra collagen amino acid sequences to the high-density collagen film could promote fibril alignment and formation, generating a more organized and

https://doi.org/10.1021/acsabm.4c01509
ACS Appl. Bio Mater. 2025, 8, 2003−2014

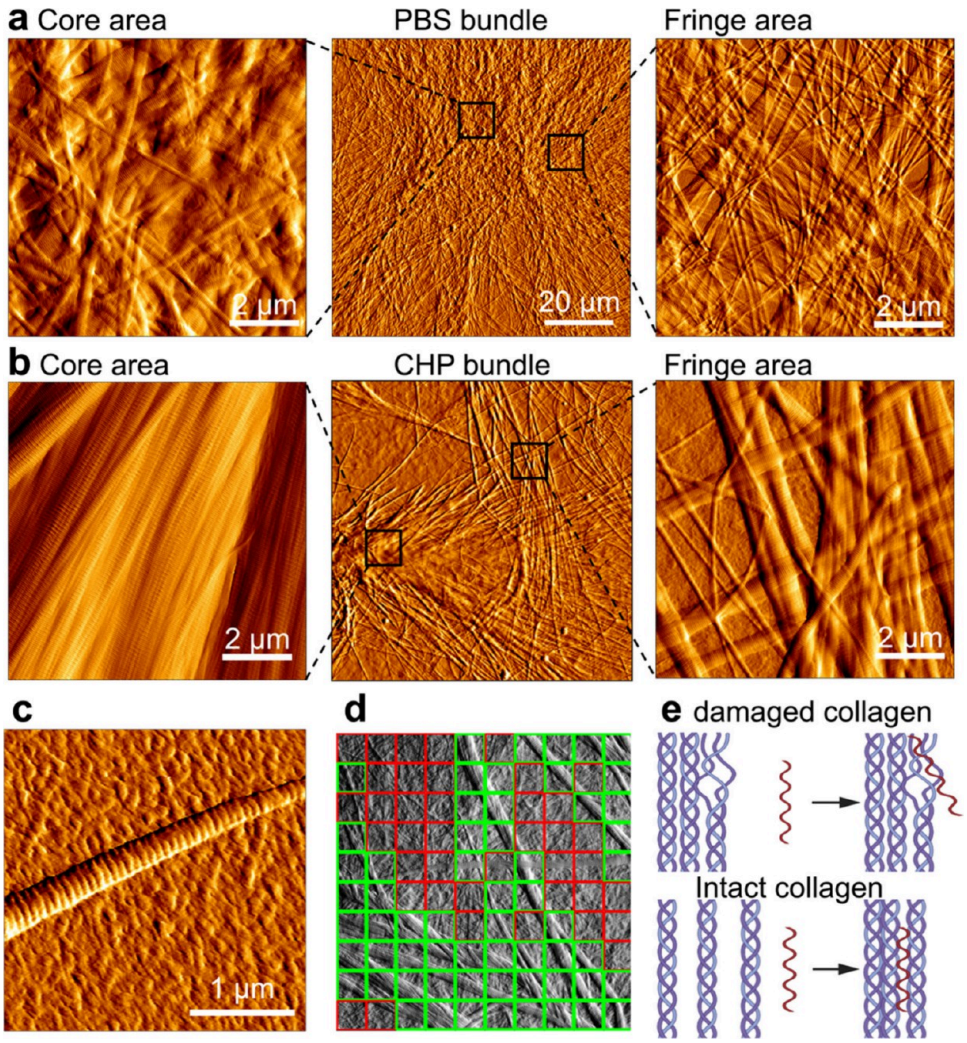

Figure 4. Morphological features of PBS and CHP-mediated collagen fibril growth. (a) AFM images of PBS-mediated collagen fibril bundles; core areas are nucleation points with densely packed, randomly organized collagen fibrils. Fringe areas have smaller fibrils that are randomly organized. (b) AFM images of CHP-mediated collagen fibril bundles; core areas are nucleation points with densely packed, highly aligned collagen fibrils. Fringe areas have smaller fibrils that are randomly organized. (c) Individual single fibrils at the extremities of the fringe area. (d) ColD recognition results in CHP-mediate collagen fibril growth. Green boxes follow collagen fibrils with 67 nm D-banding pattern, and red boxes follow the background with lactic acid-degraded amorphous collagen. (e) Proposed CHP-binding mechanism: CHP hybridizing to denatured collagen triple helices but not intact collagen fibrils in tissue (top) and binding to intact and reversible collagen molecules in high-density collagen film (bottom).

aligned collagen fiber resembling the collagen bundle observed in the tissue. CHP has the Pro-Hyp-Gly sequence with a fluorophore attached at the end, thus is an ideal candidate to investigate the effect of the collagen sequence on the formation and organization of collagen macrofibrils.

We exposed our LA-RCF to CHP (3Helix, 50 μL−1 μM) for 2 h at room temperature, and the resultant collagen structures were characterized at the macroscale by bright-field imaging and fluorescence microscopy. Whether these collagen structures are imaged by the bright-field image (20× magnification) or fluorescence microscopy, we can observe a sparse network of very large fibrils overlapping (Figure 3a). Considering that the CHP is tagged with Cy3 fluorophore at the end of the peptide,[19] we can affirm the colocation of the CHP peptides on the large fibers. This colocation suggests that the CHP is either integrated into the fibrillar structure during the fibril assembly process or becomes bound to the exterior of the fibrils postfibril assembly.

To assess the impact of CHP on collagen fibrillogenesis, time-lapse imaging of CHP-mediated fibril growth was captured every 5 min for 3 h. The PBS (non-CHP) control was captured every 10 min for 12 h (recording with 5 min intervals for 12 h generated the video file over 50 GB, due to the limitation of computer RAM and memory and the extended recording time for PBS conditions, the intervals were reduced to 10 min). An onset of collagen fibril growth was recorded 1 h after adding PBS (control) (n = 9), and the fibrils were fully formed after 8 h when no change in fibril gross morphology could be recorded any longer (Figure 3b). In contrast, the fibril growth started as early as 20 min after adding the CHP (n = 9), and the fibrils were formed entirely within 2 h. No further changes in fibril growth could be observed after that (Figure 3c). These results suggest that adding CHP to our highly dense collagen encourages fibrillogenesis by reducing the time required for fibrils to self-assemble.

https://doi.org/10.1021/acsabm.4c01509
ACS Appl. Bio Mater. 2025, 8, 2003−2014

Investigating CHP-Mediated Collagen Fibril Morphology. The morphology of these newly formed collagen macrofibrils was investigated by second harmonic generation microscopy (Figure 3d). These collagen fibrils were found to emanate from a nucleation site regardless of the presence of CHP (Figure 3d, circles). The collagen fibrils appear to grow away from this initial assembly point, forming a uniform network of large and overlapping collagen fibrils, which can be labeled collagen macrofibrils. The notion of a nucleation site is well-understood in biological systems and collagen.[43,44] Collagen fibrillogenesis typically begins when collagen molecules interact with each other and other components of the ECM.[45] This process can be influenced by cells like fibroblasts that secrete collagen precursors and other molecules that act as nucleators.[46] These sites provide an anchor that guides the orderly assembly of collagen into forming the structured fibrous networks characteristic of functional collagen. This result suggested that having anchoring sites during *in vitro* fibrillogenesis could enhance collagen fibril growth.

The macrofibrils' linearity was measured using the canny edge detection and Hough transform to identify linear structures from the PBS and CHP images,[47] highlighted in green (n = 15 for PBS and CHP) (Figure 3e). On average, 4105 linear fibrils were counted from CHP-mediated growth, and 282 linear structures were counted from the PBS control (Figure 3f). This analysis demonstrated that CHP-induced collagen fibrils had significantly more linearly arranged morphology than those from the PBS control group ($p < 0.0001$). We deduce that the presence of CHP during the self-assembly of collagen increases the rate at which these fibrils can grow and promotes a linear and directional growth of the fibrils.

To investigate the structure of these macrofibrils, we took AFM images of collagen fibrils from CHP-mediated and PBS-mediated growth. We defined two areas of interest: the area close to the nucleation point (denoted core) and several tens of micrometers away in the regions, presenting a topography resembling the bunches of wheat stalks (denoted fringe) (Figure 4a). In the case of the PBS-mediated macrofibrils, the core area comprises densely packed, randomly organized, and relatively uniform collagen fibrils with an average diameter $W_{PBS\text{-}core} = 342 \pm 110$ nm (n = 30) (Figure 4a). The fibrils in the fringe area are much smaller, with an average fibril width of $W_{PBS\text{-}fringe} = 166 \pm 34$ nm (n = 30) (Figure 4a). In the case of CHP-mediated collagen, the core area is formed of densely packed, aligned collagen fibrils that merge or fuse (Figure 4b). The cohesion of the fibrils has become such that it is impossible to distinguish neighboring fibrils within the core area. These results suggest that CHP-mediated collagen fibril growth can generate highly aligned collagen fibrils without requiring collagen cross-linking. The fringe area displayed bundles of collagen fibrils with width ranges from 155 to 670 nm (n = 30) (Figure 4b), significantly larger than those measured in the case of the PBS-mediated macrofibrils. It is possible to observe individual single fibrils at the extremities of the fringe area, ranging from 98 to 205 nm in diameter (Figure 4c).

The collagen D-banding patterns from CHP-mediated growth and PBS-mediated growth was evaluated with our ColD model, and the result showed that they both contain 67 nm D-banding patterns (n = 15). Figure 4d is a representative AFM image containing collagen fibrils and background areas with lactic acid degraded collagen. The ColD model recognizes collagen D-banding patterns similar to the ground truth, meaning that areas with fibrils are identified as "D-banding", and areas of the background are recognized as "no D-banding". This positive recognition result also confirms that the CHP-mediated collagen fibril has the structural resemblance of the native collagen with the 67 nm D-banding pattern. In summary, by adding CHP to our RCF, we observed an acceleration of collagen fibril formation through a nucleation and elongation mechanism. Furthermore, the fibril network exhibited linear and directional growth in areas with structurally aligned fibril bundles.

DISCUSSION

In this study, we created the amorphous RCF to mimic a collagen-rich environment, such as in skin or tendon, and investigate collagen fibril growth in high-density conditions using the RCF. The result indicated that increasing the collagen density from the hydrogel to a dense film can lead to doubling the size of collagen fibrils during spontaneous fibrillogenesis. Previous studies have found similar results, such as the initial collagen concentration determining the final fibril size.[48] Still, most studies were carried out on collagen fibril growth in solutions with increasing collagen concentration and measured turbidity as an indicator of collagen fibril nucleation and growth.[49,50] The collagen density in ECS is calculated to be 1.78×10^{-3} mg/mm^3 (1.78×10^{-3} mg/mL = 1.78×10^{-3} mg/mm^3), and the RCF has a collagen density of 2.67 mg/mm^3. The collagen density of skin tissue is reported to be around 1.02 mg/mm^3,.[51,52] Therefore, our RCF closely mimics the collagen density of skin tissue compared with the collagen hydrogel and can potentially serve as a better representation of the ECM than the collagen hydrogel. Observing larger fibril growth in a high collagen density further emphasizes the importance of studying collagen fibril growth in the context of collagen density that mimics collagen-rich tissue. An additional benefit of utilizing RCF to examine collagen fibril growth is observing the growth process without needing any tissue staining.

It is widely accepted that collagen molecules are incorporated into fibrils by lateral aggregation and a longitudinal stagger, yielding the characteristic collagen fibrils observed by AFM.[53] The greater availability of collagen molecules found in the collagen film (as opposed to that in the solution) would favor the lateral aggregation of collagen molecules, yielding larger fibrils. The *in vitro* type I collagen fibril assembly process depends on collagen concentration, pH, temperature, and ionic strength, whereas *in vivo*, type I collagen fibril diameter is known to be modulated by type III, type V collagen, and proteoglycans such as decorin, biglycan, and fibromodulin.[54]

In this study, we aimed to investigate the effect of CHP on collagen fibril morphology in high collagen density conditions and utilize CHP to create collagen fibril bundles that mimic the collagen fibril morphology observed in tissue, such as skin or tendon. We have demonstrated that CHP can accelerate collagen fibril growth through the nucleation and elongation mechanism and noted the structurally aligned collagen bundles influenced by CHP. The current understanding of the CHP hybridizing mechanism suggests that CHP can bind to the unwound collagen triple helix but not the intact collagen in tissue.[55] However, acid degradation does not interfere with the collagen triple helix structure.[56,57] Yet, as demonstrated by our

https://doi.org/10.1021/acsabm.4c01509
ACS Appl. Bio Mater. 2025, 8, 2003−2014

results, CHP can interact with the intact collagen molecules/fragments and influence the growth and morphology of self-assembled collagen fibrils. Consequently, we proposed a working hypothesis that CHP can interact with unwound collagen triple helix (damage detection in tissue) and intact collagen triple helix (promote fibril growth using high-density collagen film) but not with fully formed undamaged collagen fibrils in tissue (low affinity when stained with normal tissue) (Figure 4e).

The capability of CHP to hybridize with denatured collagen triple helix and detect damaged collagen in formalin-fixed tissue has been demonstrated in many publications over the past decade.[55,58,59] However, in connective tissues, collagen exists predominantly as fully formed fibrils with a minimal level of denatured triple helix, except for that damaged as part of the normal tissue remodeling. Thus, minimum CHP binding activity should be observed in normal tissues.[55] However, when tissues undergo excessive remodeling resulting from injury or disease, the presence of a denatured triple helix increases and becomes detectable through CHP hybridization. Combined with the result demonstrated with CHP and RCF previously, we propose that CHP hybridizes with denatured collagen triple helix but not the intact collagen fibrils in damaged tissue and binds to intact and reversible collagen molecules to accelerate fibril growth and alignment *in vitro*.

CHP is a short peptide with the repeat unit of Pro-Hyp-Gly, which, in our case, has been used as an accelerator for fibril growth and the generation of highly aligned collagen macrofibrils by interacting with intact collagen molecules and fragments during fibrillogenesis. To explain the mechanism of CHP-mediated collagen fibril growth, we suggest that adding exogenous Pro-Hyp-Gly (sequence of CHP) to type I collagen molecules during the fibrillogenesis results in more sites for Hyp-mediated H-bonding, more Pro-mediated helical stabilization, and stabilization through overall increase of the stereoelectronic effect, thus increasing the speed of collagen fibril growth and promoting more linearly aligned collagen fibrils.

The mechanism of how collagen fibrils could grow *in vitro* was first proposed by Wood and Keech in 1960 in which they experimented with different conditions (temperature, pH, ionic strength, and collagen concentration) for acid-soluble collagen to form fibrils and measured the rate of fibril formation through turbidimetric assay.[32,37] They have summarized the collagen fibril growth into three phases: a lag phase where no change was detected in turbidity, a growth phase where turbidity increases rapidly, and a plateau phase where the turbidity value remains constant.[32] They proposed that collagen fibrils formed during the lag phase have two steps: the first step is the formation of nuclei, and the second is the growth of fibrils from the nuclei.[37] The synthetic sequence of $(Pro\text{-}Hyp\text{-}Gly)_{10}$ (which is similar to the CHP sequence without the fluorophore) is known to self-assemble to form a higher-order structure.[60] The Brodsky Group demonstrated that $(Pro\text{-}Hyp\text{-}Gly)_{10}$ follows a nucleation growth mechanism with a lag phase, rapid growth phase, and a plateau phase similar to natural collagen fibril growth reported by Wood et al.[37,60] They then replaced the Hyp with Pro and studied $(Pro\text{-}Pro\text{-}Gly)_{10}$ self-assembly to understand the role of Hyp in self-association. They found the Pro-Pro-Gly peptide forms a much less stable triple helix and no aggregation at any temperature or concentration, emphasizing the importance of Hyp in triple helix stabilization and self-assembly.[60] They hypothesized that the Hyp hydration network likely mediates the lateral self-assembly mechanism between Hyp and the backbone carbonyl group.[60]

Collagen consists of three polypeptide chains that fold into a triple helix.[61] These chains contain repeats of the sequence Xaa-Yaa-Gly, where Xaa and Yaa residues are often Pro or Hyp.[62] The stereoelectronic effects in collagen primarily involve the conformational preferences of amino acids like Pro and Hyp, which are prevalent in their structure.[63] The stereoelectronic effects also enhance the effectiveness of hydrogen bonds within and in between the collagen molecules.[64] These bonds are critical for maintaining the integrity and strength of the helix structure and fibrils. Beyond the triple helix, collagen fibrils are formed by the lateral association of multiple helices.[43] Here, the stereoelectronic effects influence the alignment and packing of these helices through subtle electronic interactions across molecules, which dictate how well these structures can come together and stabilize the triple helix. Therefore, adding the CHP as part of our high-density collagen self-assembly process increases the stereoelectronic effects within our collagen fibrils, leading to favorable interactions that form macrofibrils.

From our observation, the macrofibril polymerization phase consisted of aggregation and elongation, where nucleation sites formed via aggregation and fibrils elongated from nucleation sites to polymerize into networks through hydrogen bonds. This observation aligns with previous work demonstrating fibril growth following aggregation and elongation processes with time-lapse liquid AFM imaging.[65] Currently, two mainstream hypotheses explain the mechanism of collagen fibril formation *in vivo*; one theory suggests that collagen molecules nucleate and grow in the axial direction, followed by side-to-side fusion and tip-to-tip fusion.[66,67] Another hypothesis describes the fibril assembling like liquid crystals that assemble spontaneously.[68,69] Our study has provided additional evidence of nucleation and side-to-side fusion to support the first fibrillogenesis hypothesis of nucleation and elongation.

Together, the data suggest that CHP mediates collagen fibril growth via lateral aggregation that generates nucleation sites, and then, the fibril elongates from the nucleation site in the longitudinal direction. CHP accelerates collagen fibril growth by integrating within fibrils and acts as a guide via hydrogen bonding, a stereoelectronic effect, and electrostatic interaction to drive the fibril alignment and growth. Our study highlights the benefit of investigating collagen fibril growth in biomimetic collagen density and the effect of CHP on creating structurally aligned collagen bundles and accelerating collagen fibril growth *in vitro*.

CONCLUSION

Our study focuses on cycling collagen self-assembly and disassembly to create a reversible collagen film, aiming to mimic the density and structural properties of native tissues. We have also utilized CNN to recognize collagen D-banding patterns at the nanoscale. For the first time, we introduced CHP to the reversible collagen film to investigate how CHP could modulate collagen fibrillogenesis. The CHPs are shown to significantly accelerate and influence the organization of collagen fibril growth compared to that of controls, leading to a more aligned and structured arrangement of fibrils. The impact of CHP suggests their role extends beyond interaction with collagen's triple helix to facilitate larger fibril assembly. Our findings underscore the potential of this method in

https://doi.org/10.1021/acsabm.4c01509
ACS Appl. Bio Mater. 2025, 8, 2003−2014

applications requiring precise collagen structure manipulation and highlight the role of biomolecular agents in directing collagen assembly dynamics. Future work could further validate the proposed working hypothesis of the CHP mechanism in collagen fibril growth, addressing the challenges associated with the clinical translation of CHP-like peptides in tissue repair and regeneration, including peptide bioavailability, long-term biostability, and potential biotoxicities. Developing more cost-effective CHP-like peptides for both *in vitro* and *in vivo* applications would significantly enhance the biomedical application of tissue repair and regeneration.

AUTHOR INFORMATION

Corresponding Author

Sophia Huang − *Matrix Functionalization and Phenotyping Lab, Faculty of Dentistry, University of Toronto, Toronto, Ontario M5G 1X3, Canada*; Email: Sophia.huang@mail.utoronto.ca

Authors

Nicole Ng − *Matrix Functionalization and Phenotyping Lab, Faculty of Dentistry, University of Toronto, Toronto, Ontario M5G 1X3, Canada*

Mina Vaez − *Matrix Functionalization and Phenotyping Lab, Faculty of Dentistry, University of Toronto, Toronto, Ontario M5G 1X3, Canada*

Boris Hinz − *Laboratory of Tissue Repair and Regeneration, Keenan Research Institute for Biomedical Science of the St. Michael's Hospital, Toronto, Ontario M5B 1M4, Canada*

Iona Leong − *Department of Pathology and Laboratory Medicine, Mount Sinai Hospital, Toronto, Ontario M5G 1X5, Canada; Department of Oral Pathology and Oral Medicine, Faculty of Dentistry, University of Toronto, Toronto, Ontario M5G 1X3, Canada*

Laurent Bozec − *Matrix Functionalization and Phenotyping Lab, Faculty of Dentistry, University of Toronto, Toronto, Ontario M5G 1X3, Canada*

Complete contact information is available at: https://pubs.acs.org/10.1021/acsabm.4c01509

Author Contributions

S.H. and L.B. conceptualized the work and designed the study. S.H., N.N., and M.V. performed the experiments. S.H. performed the coding and conducted the literature search. I.L. and B.H. provided advisory support for the project. S.H. prepared the initial draft of the manuscript, with all authors actively participating in the refinement and finalization of the manuscript through comprehensive review and contributions. L.B. supervised the project.

Notes

The authors declare no competing financial interest.

ACKNOWLEDGMENTS

This work was supported by a grant from the Matrix Functionalization & Phenotyping Lab (Bozec-lab), Natural Sciences and Engineering Research Council of Canada (NSERC) Discovery Award (RGPIN-2021-02694), Ontario Research Fund (ORF) Award (RE010-068), and The Network for Canadian Oral Health Research (NCHOR) award (NFSG2019-03). The research of B.H. is supported by a foundation grant (#375597) and project grant (#190081) from the Canadian Institutes of Health Research and support from the John Evans Leadership funds (#36050 and #38861) and innovation funds ('Fibrosis Network, #36349') from the Canada Foundation for Innovation (CFI) and the ORF. We acknowledge the Collaborative Advanced Microscopy Laboratories of Dentistry (CAMiLoD), Dhaarmini Rajshankar, and the Faculty of Dentistry (University of Toronto, Toronto, ON, Canada) for service, training, and expert advice received with atomic force microscopy imaging. We thank the Cell and System Biology Department Imaging Facility (University of Toronto, Toronto, ON, Canada), Dr. Kenana Al Kakouni, and Dr. Sergey Plotnikov for the service, training, and expert advice received with second harmonics generation imaging. We thank Dr. Nancy Forde (Department of Physics, Simon Fraser University, Burnaby, BC, Canada) for her expert advice on collagen hybridizing peptide usage and application.

REFERENCES

(1) Muncie, J. M.; Weaver, V. M. The Physical and Biochemical Properties of the Extracellular Matrix Regulate Cell Fate. *Curr. Top Dev Biol.* **2018**, *130*, 1.

(2) Amirrah, I. N.; Lokanathan, Y.; Zulkiflee, I.; Wee, M. F. M. R.; Motta, A.; Fauzi, M. B. A Comprehensive Review on Collagen Type I Development of Biomaterials for Tissue Engineering: From Biosynthesis to Bioscaffold. *Biomedicines* **2022**, *10* (9), 2307.

(3) Shoulders, M. D.; Raines, R. T. Collagen Structure and Stability. *Annu. Rev. Biochem.* **2009**, *78*, 929.

(4) Exposito, J. Y.; Valcourt, U.; Cluzel, C.; Lethias, C. The Fibrillar Collagen Family. *Int. J. Mol. Sci.* **2010**, *11* (2), 407.

(5) Kar, K.; Wang, Y.-H.; Brodsky, B. Sequence Dependence of Kinetics and Morphology of Collagen Model Peptide Self-Assembly into Higher Order Structures. *Protein Sci.* **2008**, *17* (6), 1086.

(6) Kadler, K. E.; Holmes, D. F.; Trotter, J. A.; Chapman, J. A. Collagen Fibril Formation. *Biochem. J.* **1996**, *316*, 1−11.

(7) Petruska, J. A.; Hodge, A. J. A Subunit Model for the Tropocollagen Macromolecule. *Biochemistry* **1964**, *51*, 871.

(8) Sorushanova, A.; Delgado, L. M.; Wu, Z.; Shologu, N.; Kshirsagar, A.; Raghunath, R.; Mullen, A. M.; Bayon, Y.; Pandit, A.; Raghunath, M.; Zeugolis, D. I. The Collagen Suprafamily: From Biosynthesis to Advanced Biomaterial Development. *Adv. Mater.* **2019**, *31* (1), e1801651.

(9) Lu, P.; Ruan, D.; Huang, M.; Tian, M.; Zhu, K.; Gan, Z.; Xiao, Z. Harnessing the Potential of Hydrogels for Advanced Therapeutic Applications: Current Achievements and Future Directions. *Signal Transduction Targeted Therapy* **2024**, *9* (1), 1−66.

(10) Amirrah, I. N.; Lokanathan, Y.; Zulkiflee, I.; Wee, M. F. M. R.; Motta, A.; Fauzi, M. B. A Comprehensive Review on Collagen Type I Development of Biomaterials for Tissue Engineering: From Biosynthesis to Bioscaffold. *Biomedicines* **2022**, *10* (9), 2307.

(11) Wang, H. A Review of the Effects of Collagen Treatment in Clinical Studies. *Polymers (Basel)* **2021**, *13* (22), 3868.

(12) Mathew-Steiner, S. S.; Roy, S.; Sen, C. K. Collagen in Wound Healing. *Bioengineering* **2021**, *8* (5), 63.

(13) Chattopadhyay, S.; Raines, R. T. Review Collagen-Based Biomaterials for Wound Healing. *Biopolymers* **2014**, *101* (8), 821−833.

(14) Zhou, N.; Liu, Y. Da; Zhang, Y.; Gu, T. W.; Peng, L. H. Pharmacological Functions, Synthesis, and Delivery Progress for Collagen as Biodrug and Biomaterial. *Pharmaceutics* **2023**, *15* (5), 1443.

(15) Patil, V. A.; Masters, K. S. Engineered Collagen Matrices. *Bioengineering* **2020**, *7* (4), 163.

(16) Xu, Y.; Kirchner, M. Collagen Mimetic Peptides. *Bioengineering* **2021**, *8*, 5.

(17) O'Leary, L. E. R.; Fallas, J. A.; Bakota, E. L.; Kang, M. K.; Hartgerink, J. D. Multi-Hierarchical Self-Assembly of a Collagen Mimetic Peptide from Triple Helix to Nanofibre and Hydrogel. *Nat. Chem.* **2011**, *3* (10), 821−828.

(18) McGuinness, K.; Khan, I. J.; Nanda, V. Morphological Diversity and Polymorphism of Self-Assembling Collagen Peptides Controlled by Length of Hydrophobic Domains. *ACS Nano* **2014**, *8* (12), 12514−12523.
(19) Hwang, J.; Huang, Y.; Burwell, T. J.; Peterson, N. C.; Connor, J.; Weiss, S. J.; Yu, S. M.; Li, Y. In Situ Imaging of Tissue Remodeling with Collagen Hybridizing Peptides. *ACS Nano* **2017**, *11* (10), 9825−9835.
(20) Li, Y.; Yu, S. M. In Situ Detection of Degraded and Denatured Collagen via Triple Helical Hybridization: New Tool in Histopathology. *Methods Mol. Biol.* **2019**, *1944*, 135−144.
(21) Schroeder, A. B.; Karim, A.; Ocotl, E.; Dones, J. M.; Chacko, J. V.; Liu, A.; Raines, R. T.; Gibson, A. L. F.; Eliceiri, K. W. Optical Imaging of Collagen Fiber Damage to Assess Thermally Injured Human Skin. *Wound Repair Regen* **2020**, *28* (6), 848−855.
(22) Vasse, G. F.; Van Os, L.; De Jager, M.; Jonker, M. R.; Borghuis, T.; Van Den Toorn, L. T.; Jellema, P.; White, E. S.; Van Rijn, P.; Harmsen, M. C.; Heijink, I. H.; Melgert, B. N.; Burgess, J. K. Adipose Stromal Cell-Secretome Counteracts Profibrotic Signals From IPF Lung Matrices. *Front Pharmacol* **2021**, *12*, na DOI: 10.3389/fphar.2021.669037.
(23) Kwa, K. A. A.; van Haasterecht, L.; Elgersma, A.; Breederveld, R. S.; Groot, M. L.; van Zuijlen, P. P. M.; Boekema, B. K. H. L. Effective Enzymatic Debridement of Burn Wounds Depends on the Denaturation Status of Collagen. *Wound Repair Regen* **2020**, *28* (5), 666−675.
(24) Brown, R. A.; Wiseman, M.; Chuo, C. B.; Cheema, U.; Nazhat, S. N. Ultrarapid Engineering of Biomimetic Materials and Tissues: Fabrication of Nano- and Microstructures by Plastic Compression. *Adv. Funct Mater.* **2005**, *15* (11), 1762−1770.
(25) Chen, X.; Nadiarynkh, O.; Plotnikov, S.; Campagnola, P. J. Second Harmonic Generation Microscopy for Quantitative Analysis of Collagen Fibrillar Structure. *Nature Protocols* **2012**, *7* (4), 654−669.
(26) Geckil, H.; Xu, F.; Zhang, X.; Moon, S.; Demirci, U. Engineering Hydrogels as Extracellular Matrix Mimics. *Nanomedicine (Lond)* **2010**, *5* (3), 469.
(27) Cheema, U.; Brown, R. A. Rapid Fabrication of Living Tissue Models by Collagen Plastic Compression: Understanding Three-Dimensional Cell Matrix Repair In Vitro. *Adv. Wound Care (New Rochelle)* **2013**, *2* (4), 176.
(28) Abou Neel, E. A.; Bozec, L.; Knowles, J. C.; Syed, O.; Mudera, V.; Day, R.; Hyun, J. K. Collagen — Emerging Collagen Based Therapies Hit the Patient. *Adv. Drug Deliv Rev.* **2013**, *65* (4), 429−456.
(29) Huang, S.; Strange, A.; Maeva, A.; Siddiqui, S.; Bastien, P.; Aguayo, S.; Vaez, M.; Montagu-Pollock, H.; Ghibaudo, M.; Potter, A.; Pageon, H.; Bozec, L. Quantitative Nanohistology of Aging Dermal Collagen. *Frontiers in Aging* **2023**, *4*, na DOI: 10.3389/fragi.2023.1178566.
(30) Gross, J.; Schmitt, F. O. The Structure of Human Skin Collagen as Studied with the Electron Microscope. *J. Exp Med.* **1948**, *88* (5), 555−568.
(31) Chang, J.; Garva, R.; Pickard, A.; Yeung, C. Y. C.; Mallikarjun, V.; Swift, J.; Holmes, D. F.; Calverley, B.; Lu, Y.; Adamson, A.; Raymond-Hayling, H.; Jensen, O.; Shearer, T.; Meng, Q. J.; Kadler, K. E. Circadian Control of the Secretory Pathway Maintains Collagen Homeostasis. *Nat. Cell Biol.* **2020**, *22* (1), 74.
(32) Wood, G. C.; Keech, M. K. The Formation of Fibrils from Collagen Solutions 1. The Effect of Experimental Conditions: Kinetic and Electron-Microscope Studies. *Biochem. J.* **1960**, *75*, 588.
(33) Bak, S. Y.; Lee, S. W.; Choi, C. H.; Kim, H. W. Assessment of the Influence of Acetic Acid Residue on Type I Collagen during Isolation and Characterization. *Materials* **2018**, *11* (12), 2518.
(34) Li, X.; Yang, Y.; Zhang, B.; Lin, X.; Fu, X.; An, Y.; Zou, Y.; Wang, J. X.; Wang, Z.; Yu, T. Lactate Metabolism in Human Health and Disease. *Signal Transduct Target Ther* **2022**, *7* (1), 305.
(35) Bozec, L.; Odlyha, M. Thermal Denaturation Studies of Collagen by Microthermal Analysis and Atomic Force Microscopy. *Biophysj* **2011**, *101*, 228−236.
(36) Vaez, M.; Asgari, M.; Hirvonen, L.; Bakir, G.; Khattignavong, E.; Ezzo, M.; Aguayo, S.; Schuh, C. M.; Gough, K.; Bozec, L. Modulation of the Biophysical and Biochemical Properties of Collagen by Glycation for Tissue Engineering Applications. *Acta Biomater* **2023**, *155*, 182−198.
(37) Wood, G. C. The Formation of Fibrils from Collagen Solutions. 2. A Mechanism for Collagen-Fibril Formation. *Biochem. J.* **1960**, *75* (3), 605.
(38) *Gwyddion - Free SPM (AFM, SNOM/NSOM, STM, MFM, . . .) data analysis software*. http://gwyddion.net/ (accessed 2024−08−12).
(39) Baranwal, N.; Doravari, P.; Kachhoria, R. Classification of Histopathology Images of Lung Cancer Using Convolutional Neural Network (CNN). *Disruptive Developments in Biomedical Applications* **2022**, 75.
(40) Haggenmüller, S.; Maron, R. C.; Hekler, A.; Utikal, J. S.; Barata, C.; Barnhill, R. L.; Beltraminelli, H.; Berking, C.; Betz-Stablein, B.; Blum, A.; Braun, S. A.; Carr, R.; Combalia, M.; Fernandez-Figueras, M. T.; Ferrara, G.; Fraitag, S.; French, L. E.; Gellrich, F. F.; Ghoreschi, K.; Goebeler, M.; Guitera, P.; Haenssle, H. A.; Haferkamp, S.; Heinzerling, L.; Heppt, M. V.; Hilke, F. J.; Hobelsberger, S.; Krahl, D.; Kutzner, H.; Lallas, A.; Liopyris, K.; Llamas-Velasco, M.; Malvehy, J.; Meier, F.; Müller, C. S. L.; Navarini, A. A.; Navarrete-Dechent, C.; Perasole, A.; Poch, G.; Podlipnik, S.; Requena, L.; Rotemberg, V. M.; Saggini, A.; Sangueza, O. P.; Santonja, C.; Schadendorf, D.; Schilling, B.; Schlaak, M.; Schlager, J. G.; Sergon, M.; Sondermann, W.; Soyer, H. P.; Starz, H.; Stolz, W.; Vale, E.; Weyers, W.; Zink, A.; Krieghoff-Henning, E.; Kather, J. N.; von Kalle, C.; Lipka, D. B.; Fröhling, S.; Hauschild, A.; Kittler, H.; Brinker, T. J. Skin Cancer Classification via Convolutional Neural Networks: Systematic Review of Studies Involving Human Experts. *Eur. J. Cancer* **2021**, *156*, 202−216.
(41) Howard, A. G.; Zhu, M.; Chen, B.; Kalenichenko, D.; Wang, W.; Weyand, T.; Andreetto, M. MobileNets: Efficient Convolutional Neural Networks for Mobile Vision Applications. *arXiv Preprint*, arXiv:1704.04861, 2017. DOI: 10.48550/arXiv.1704.04861
(42) Darvish, D. M. Collagen Fibril Formation in Vitro: From Origin to Opportunities. *Mater. Today Bio* **2022**, *15*, 100322.
(43) Shoulders, M. D.; Raines, R. T. Collagen Structure and Stability. *Annu. Rev. Biochem.* **2009**, *78*, 929.
(44) Holmes, D. F.; Tait, A.; Hodson, N. W.; Sherratt, M. J.; Kadler, K. E. Growth of Collagen Fibril Seeds from Embryonic Tendon: Fractured Fibril Ends Nucleate New Tip Growth. *J. Mol. Biol.* **2010**, *399* (1), 9−16.
(45) Musiime, M.; Chang, J.; Hansen, U.; Kadler, K. E.; Zeltz, C.; Gullberg, D. Collagen Assembly at the Cell Surface: Dogmas Revisited. *Cells* **2021**, *10* (3), 662.
(46) Kadler, K. E.; Hill, A.; Canty-Laird, E. G. Collagen Fibrillogenesis: Fibronectin, Integrins, and Minor Collagens as Organizers and Nucleators. *Curr. Opin Cell Biol.* **2008**, *20* (5−24), 495.
(47) Nejim, Z.; Navarro, L.; Morin, C.; Badel, P. Quantitative Analysis of Second Harmonic Generated Images of Collagen Fibers: A Review. *Research on Biomedical Engineering* **2023**, *39*, 273.
(48) Gobeaux, F.; Mosser, G.; Anglo, A.; Panine, P.; Davidson, P.; Giraud-Guille, M. M.; Belamie, E. Fibrillogenesis in Dense Collagen Solutions: A Physicochemical Study. *J. Mol. Biol.* **2008**, *376* (5), 1509−1522.
(49) Silver, F. H.; Birk, D. E. Kinetic Analysis of Collagen Fibrillogenesis: I. Use of Turbidity-Time Data. *Coll Relat Res.* **1983**, *3* (5), 393−405.
(50) Mosser, G.; Anglo, A.; Helary, C.; Bouligand, Y.; Giraud-Guille, M. M. Dense Tissue-like Collagen Matrices Formed in Cell-Free Conditions. *Matrix Biol.* **2006**, *25* (1), 3−13.
(51) Liang, X.; Boppart, S. A. Biomechanical Properties of In Vivo Human Skin From Dynamic Optical Coherence Elastography. *IEEE Trans Biomed Eng.* **2010**, *57* (4), 953.

(52) Oikarinen, A. Aging of the Skin Connective Tissue: How to Measure the Biochemical and Mechanical Properties of Aging Dermis. *Photodermatol Photoimmunol Photomed* **1994**, *10*, 47−52.
(53) Cisneros, D. A.; Hung, C.; Franz, C. M.; Muller, D. J. Observing Growth Steps of Collagen Self-Assembly by Time-Lapse High-Resolution Atomic Force Microscopy. *J. Struct Biol.* **2006**, *154* (3), 232−245.
(54) Sirotkina, M. Y.; Nashchekina, Y. A. Collagen Fibrils of Various Diameters: Formation Conditions and Principles of Functioning. *Cell tissue biol* **2022**, *16* (6), 513−520.
(55) Li, X.; Zhang, Q.; Yu, S. M.; Li, Y. The Chemistry and Biology of Collagen Hybridization. *J. Am. Chem. Soc.* **2023**, *145*, 10901−10916.
(56) Bak, S. Y.; Lee, S. W.; Choi, C. H.; Kim, H. W. Assessment of the Influence of Acetic Acid Residue on Type I Collagen during Isolation and Characterization. *Materials* **2018**, *11* (12), 2518.
(57) Davison, P. F.; Cannon, D. J.; Andersson, L. P. The Effects of Acetic Acid on Collagen Cross-Links. *Connect Tissue Res.* **1972**, *1* (3), 205−216.
(58) Marino, M.; Converse, M. I.; Monson, K. L.; Wriggers, P. Molecular-Level Collagen Damage Explains Softening and Failure of Arterial Tissues: A Quantitative Interpretation of CHP Data with a Novel Elasto-Damage Model. *J. Mech Behav Biomed Mater.* **2019**, *97*, 254−271.
(59) Bennink, L. L.; Li, Y.; Kim, B.; Shin, I. J.; San, B. H.; Zangari, M.; Yoon, D.; Yu, S. M. Visualizing Collagen Proteolysis by Peptide Hybridization: From 3D Cell Culture to in Vivo Imaging. *Biomaterials* **2018**, *183*, 67−76.
(60) Kar, K.; Amin, P.; Bryan, M. A.; Persikov, A. V.; Mohs, A.; Wang, Y.-H.; Brodsky, B. Self-Association of Collagen Triple Helix Peptides into Higher Order Structures * □ S. *J. Biol. Chem.* **2006**, *281* (44), 33283−33290.
(61) Ramachandran, G. N.; Kartha, G. Structure of Collagen. *Nature 1954 174:4423* **1954**, *174* (4423), 269−270.
(62) Brodsky, B.; Ramshaw, J. A.M. The Collagen Triple-Helix Structure. *Matrix Biology* **1997**, *15*, 545−554.
(63) Bretscher, L. E.; Jenkins, C. L.; Taylor, K. M.; DeRider, M. L.; Raines, R. T. Conformational Stability of Collagen Relies on a Stereoelectronic Effect [23]. *J. Am. Chem. Soc.* **2001**, *123* (4), 777−778.
(64) Hodges, J. A.; Raines, R. T. Stereoelectronic Effects on Collagen Stability: The Dichotomy of 4-Fluoroproline Diastereomers. *J. Am. Chem. Soc.* **2003**, *125* (31), 9262−9263.
(65) Franz, C. M.; Muller, D. J. Studying Collagen Self-Assembly by Time-Lapse High-Resolution Atomic Force Microscopy. *Methods Mol. Biol.* **2011**, *736*, 97−107.
(66) Fang, M.; Goldstein, E. L.; Turner, A. S.; Les, C. M.; Orr, B. G.; Fisher, G. J.; Welch, K. B.; Rothman, E. D.; Banaszak Holl, M. M. Type I Collagen D-Spacing in Fibril Bundles of Dermis, Tendon and Bone: Bridging Between Nano- and Micro-Level Tissue Hierarchy. *ACS Nano* **2012**, *6* (11), 9503.
(67) Canty, E. G.; Kadler, K. E. Procollagen Trafficking, Processing and Fibrillogenesis. *J. Cell Sci.* **2005**, *118* (7), 1341−1353.
(68) Gobeaux, F.; Mosser, G.; Anglo, A.; Panine, P.; Davidson, P.; Giraud-Guille, M. M.; Belamie, E. Fibrillogenesis in Dense Collagen Solutions: A Physicochemical Study. *J. Mol. Biol.* **2008**, *376* (5), 1509−1522.
(69) Giraud-Guille, M. M. Liquid Crystallinity in Condensed Type I Collagen Solutions. A Clue to the Packing of Collagen in Extracellular Matrices. *J. Mol. Biol.* **1992**, *224* (3), 861−873.

https://doi.org/10.1021/acsabm.4c01509
ACS Appl. Bio Mater. 2025, 8, 2003−2014